RSC Advances

ROYAL SOCIETY OF CHEMISTRY

www.rsc.org/advances

RSC Advances

Cite this: DOI: 10.1039/c0xx00000x

PAPER

www.rsc.org/xxxxxx

Approach to tune short-circuit current and open-circuit voltage of dye-sensitized solar cells: π-linker modification and photoanode selection†

Shengbo Zhu,[a] Zhongwei An,*[a,b] Xinbing Chen,[a] Pei Chen[a] and Qianfeng Liu[c]

Received (in XXX, XXX) Xth XXXXXXXXX 20XX, Accepted Xth XXXXXXXXX 20XX

DOI: 10.1039/b000000x

The modification of π-linkers represents a viable strategy to improve the performance of organic dye in dye-sensitized solar cells (DSSCs). On the basis of the π-linker modification, four cyclic thiourea functionalized dyes (**AZ260**, **AZ261**, **AZ262**, and **AZ263**) were synthesized and their effects on the short-circuit current density (J_{sc}) and open-circuit voltage (V_{oc}) were investigated. The results showed that **AZ261** bearing a *n*-hexyl chain on the π-linker generated higher J_{sc} (16.02 mA cm^{-2}) and V_{oc} (739.4 mV) than those of **AZ6** without substituent on the bithiophene (J_{sc} = 15.89 mA cm^{-2}, V_{oc} = 729.2 mV, PCE = 7.20%), and a higher PCE of 7.42% was obtained from **AZ261**. Further insertion of a double-bond into the π-linker (**AZ263**) yielded the highest J_{sc} (17.83 mA cm^{-2}) with the somewhat lower V_{oc} (719.2 mV), and delivered the highest PCE up to 8.24%. In addition, the function of mesoporous spherical TiO_2 on the photoanodes were also systematically examined and proved to be beneficial to increase the J_{sc}.

1. Introduction

Since the pioneer work reported by O'Regan and Grätzel in 1991,[1] significant advances have been made in dye-sensitized solar cells (DSSCs). As the key component of DSSCs, sensitizers have evolved into two general classes: metal-complex sensitizers and organic sensitizers.[2] Organic sensitizers have attracted ever-increasing attention due to their unique advantages such as facile modification and purification, readily available raw materials, low cost, and high molar extinction coefficients compared to metal-complex sensitizers.[3] DSSCs based on organic sensitizers have reached the power conversion efficiency (PCE) of ~10%,[4] which needs to be further improved. Therefore, how to enhance the PCE of DSSCs becomes a philosophic strategy. Under a given incident illumination intensity (P_{in}), the PCE of a cell is defined as the short-circuit current density (J_{sc}), the open-circuit voltage (V_{oc}), and the fill factor (FF), as follows:[5]

$$\mathrm{PCE} = \frac{J_{sc} V_{oc} \mathrm{FF}}{P_{in}}$$

Obviously, high values of J_{sc} and V_{oc} are critical to improve the PCE. There are many factors that can affect the J_{sc}, such as light absorption range of sensitizers, sensitizer-loading capacity on TiO_2 photoanodes and scattering layers.[6,7] The V_{oc} is determined by the difference between the Fermi-level of the TiO_2 and the redox level of the redox couple in the electrolyte.[8] Under the same assembling conditions, however, the different V_{oc} values are more likely determined by the differences in electron lifetimes[9] or recombination rates.[10] Therefore, further structural optimization of organic sensitizers and selection of the materials used in DSSCs fabrication for high J_{sc} and V_{oc} are challenges. With this in mind, our previous work [11] reported the cyclic thiourea functionalized triphenylamine as donor to construct the dye molecules. The dyes containing such donor displayed a high J_{sc} combined with a high V_{oc} due to their broad light absorption band and suppression of dye aggregations. We found that the π-linkers have a significant effect on the J_{sc} and V_{oc}. Several dye substrates are valuable, which contain the thiophene as the π-linker and generally exhibit high J_{sc} and limiting V_{oc}.[9] The high J_{sc} might be explained by the prominent electron-transport properties of the bithiophene[12,13] and the broad absorption band, while the low V_{oc} may be caused by the shorter electron lifetimes from the DSSCs.[14] It was reported that the introduction of alkyl chains can effectively inhibit the intermolecular π-π aggregation [15] and electron recombination for the purpose of reducing voltage losses,[16] however, the remarkable molecular twist because of the strong steric hindrance in the conjugated unit will weaken the conjugation, and thus make the maximum absorption wavelength (λ_{max}) blue-shift.[9,17] On the other hand, one double-bond insertion between triphenylamine and thiophene units brings up the J_{sc} and down the V_{oc}.[18] In this study, our effort to improve the J_{sc} and V_{oc} by the modification of the bithiophene linkers is described. Four dyes containing cyclic thiourea functionalized triphenylamine as

[a] *Key Laboratory of Applied Surface and Colloid Chemistry, School of Materials Science and Engineering, Shaanxi Normal University, Xi'an 710062, China. E-mail: gmecazw@163.com; Fax: +86 29 8153 0702; Tel: +86 29 8153 0720*

[b] *Xi'an Modern Chemistry Research Institute, Xi'an 710065, China.*

[c] *Xi'an Ruilian Modern Electronic Chemicals Co. Ltd., Xi'an 710077, China.*

† Electronic Supplementary Information (ESI) available: Synthetic details of intermediates, characterizations, and additional experimental data. See DOI: 10.1039/b000000x/

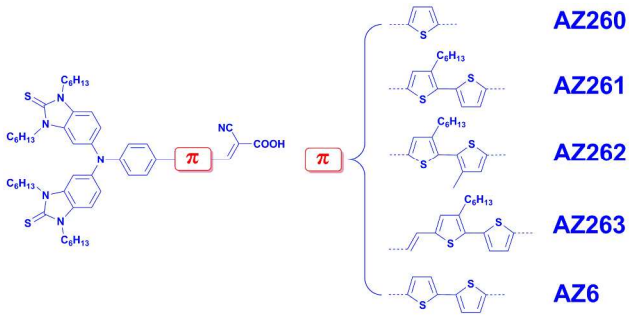

Fig. 1 Chemical structures of **AZ260-263** and **AZ6**. Herein C_6H_{13} denotes *n*-hexyl.

donors and thiophene/bithiophene as π-linkers (**AZ260**, **AZ261**, **AZ262** and **AZ263** of Fig. 1) were designed and synthesized, and their DSSC performances were evaluated as well, with an objective to exert the advantages and remedy the shortages of bithiophenes as conjugated units. Besides, the effect of the mesoporous spherical TiO_2 [19] overlayer on the photovoltaic properties was also examined.

2. Experimental

2.1. Materials

All chemicals and solvents were purchased from Aladdin-reagent Co. and Sinopharm Chemical Reagent Co. and used without further purification unless stated otherwise. THF was dried by sodium before use. The synthetic routes of **AZ260-263** are shown in Scheme 1. The synthesis of starting materials **1** and **5** were reported in our previous paper,[11] and the synthetic details of intermediates **2**, **3-a**, **3-b**, **3-c**, **4-a**, **4-b**, **4-c**, **6**, and **7** are described in the ESI†. The synthesis procedures of **AZ260-263** are described below.

General synthesis procedure of AZ260-263.

In a 50 mL 3-necked flask, the compound **4-a**, **4-b**, **4-c** or **7** (0.70 mmol), acetic acid (50 mL), cyanoacetic acid (1.75 mmol) and ammonium acetate (2.10 mmol) were added in turn under a nitrogen atmosphere. The reaction mixture was refluxed for 5 h. After cooling to room temperature, the mixture was poured into ice water. The precipitate was filtered, washed by distilled water, and purified by column chromatography (silica gel, 200-300 mesh; PE-DCM mixture as the eluent; where PE is petroleum ether, and DCM is dichloromethane) to obtain the product **AZ260-263** as a dark purple solid.

AZ260. Yield: 65.7%. ^{1}H NMR (400 MHz, $CDCl_3$): δ (ppm) 8.31 (s, 1H), 7.77 (d, *J* = 4.8 Hz, 1H), 7.58 (d, *J* = 10.8 Hz, 2H), 7.35 (d, *J* = 4.4 Hz, 1H), 7.13 (d, *J* = 11.2 Hz, 2H), 7.03-7.00 (m, 6H), 4.29 (t, *J* = 7.6 Hz, 4H), 4.20 (t, *J* = 8.8 Hz, 4H), 1.84-1.82 (m, 4H), 1.76-1.74 (m, 4H), 1.44-1.26 (m, 24H), 0.89 (t, *J* = 8.8 Hz, 6H), 0.82 (t, *J* = 8.8 Hz, 6H). ^{13}C NMR (100 MHz, $CDCl_3$): δ (ppm) 168.65, 166.95, 155.01, 148.83, 146.69, 141.42, 139.48, 132.77, 132.17, 128.27, 126.58, 124.44, 122.34, 119.93, 119.82, 114.83, 108.74, 105.47, 94.86, 43.94, 43.75, 30.45, 30.37, 26.91, 26.79, 25.56, 25.43, 21.52, 21.44, 12.99, 12.96. MS (ESI) *m/z* calcd. for $C_{52}H_{66}N_6O_2S_3$: 902.44. Found: 901.43 ([M-H]$^-$). Anal. Calcd. for $C_{52}H_{66}N_6O_2S_3$: C, 69.14; H, 7.36; N, 9.30. Found: C, 69.07; H, 7.41; N, 9.23.

AZ261. Yield: 83.4%. ^{1}H NMR (400 MHz, $CDCl_3$): δ (ppm) 8.30 (s, 1H), 7.78 (d, *J* = 4.4 Hz,1H), 7.48 (d, *J* = 8.8 Hz, 2H), 7.26 (d, *J* = 4.0 Hz, 1H), 7.12 (s, 1H), 7.10 (d, *J* = 8.8 Hz, 2H), 7.04-6.97 (m, 6H), 4.28 (t, *J* = 7.6 Hz, 4H), 4.19 (t, *J* = 7.2 Hz, 4H), 2.85 (t, *J* = 7.8 Hz, 2H), 1.87-1.80 (m, 4H), 1.78-1.67 (m, 6H), 1.50-1.41 (m, 6H), 1.37-1.22 (m, 24H), 0.89 (t, *J* = 7.2 Hz, 9H), 0.83 (t, *J* = 7.0 Hz, 6H). ^{13}C NMR (100 MHz, $CDCl_3$): δ (ppm) 169.40, 167.88, 148.38, 148.32, 147.19, 144.78, 144.26, 143.03, 138.34, 134.18, 133.13, 128.86, 128.13, 127.40, 126.64, 126.00, 125.88, 121.88, 120.46, 115.84, 109.67, 106.05, 96.11, 44.94, 44.74, 31.67, 31.48, 31.42, 30.61, 30.20, 29.48, 27.94, 27.82, 26.58, 26.45, 22.59, 22.55, 22.48, 14.09, 14.03, 14.01. MS (ESI) *m/z* calcd. for $C_{62}H_{80}N_6O_2S_4$: 1068.52. Found: 1067.51 ([M-H]$^-$). Anal. Calcd. for $C_{62}H_{80}N_6O_2S_4$: C, 69.62; H, 7.54; N, 7.86. Found: C, 69.56; H, 7.48; N, 7.94.

AZ262. Yield: 85.8. ^{1}H NMR (400 MHz, $CDCl_3$): δ (ppm) 8.27 (s, 1H), 7.70 (s, 1H), 7.48 (d, *J* = 8.8 Hz, 2H), 7.14 (s, 1H), 7.10 (d, *J* = 8.8 Hz, 2H), 7.05-6.97 (m, 6H), 4.28 (t, *J* = 7.6 Hz, 4H), 4.19 (t, *J* = 7.2 Hz, 4H), 2.60 (t, *J* = 7.6 Hz, 2H), 2.30 (s, 3H), 1.87-1.80 (m, 4H), 1.77-1.70 (m, 4H), 1.64-1.57 (m, 2H), 1.48-1.41 (m, 6H), 1.36-1.24 (m, 24H), 0.89 (t, *J* = 6.8 Hz, 6H), 0.85-0.81 (m, 9H). ^{13}C NMR (100 MHz, $CDCl_3$): δ (ppm) 169.33, 167.40, 148.06, 145.12, 144.59, 143.22, 142.16, 140.59, 139.07, 138.31, 134.36, 133.11, 128.73, 127.43, 126.40, 125.67, 124.45, 122.24, 120.31, 115.76, 109.64, 105.88, 97.68, 44.94, 44.73, 31.57, 31.48, 31.42, 30.61, 29.70, 29.23, 29.04, 27.95, 27.82, 26.58, 26.45, 22.55, 22.48, 14.95, 14.07, 14.03, 14.00. MS (ESI) *m/z* calcd. for $C_{63}H_{82}N_6O_2S_4$: 1082.53. Found: 1081.52 ([M-H]$^-$). Anal. Calcd. for $C_{63}H_{82}N_6O_2S_4$: C, 69.83; H, 7.63; N, 7.76. Found: C, 69.79; H, 7.51; N, 7.83.

AZ263. Yield: 79.5%. ^{1}H NMR (400 MHz, $CDCl_3$): δ (ppm) 8.19(s, 1H), 7.68 (d, *J* = 4.4 Hz, 1H), 7.27 (d, *J* = 8.4 Hz, 2H), 7.16 (d, *J* = 4.4 Hz, 1H), 7.01 (d, *J* = 16.0 Hz, 1H), 6.98 (s, 1H), 6.93-6.88(m, 8H), 6.83 (d, *J* = 16.0 Hz, 1H), 4.19 (t, *J* = 7.6 Hz, 4H), 4.10 (t, *J* = 7.4 Hz, 4H), 2.72 (t, *J* = 7.6 Hz, 2H), 1.78-1.71 (m, 4H), 1.69-1.56 (m, 6H), 1.41-1.31 (m, 6H), 1.29-1.15 (m, 24H), 0.81 (t, *J* = 7.0 Hz, 9H), 0.75 (t, *J* = 7.0 Hz, 6H). ^{13}C NMR (100 MHz, $CDCl_3$): δ (ppm) 168.33, 166.65, 147.17, 147.14, 146.03, 142.96, 142.77, 142.13, 138.09, 133.22, 132.07, 129.17, 128.70, 128.63, 127.75, 126.95, 126.55, 124.89, 120.85, 119.39, 118.16, 114.83, 108.59, 104.96, 95.13, 43.91, 43.70, 30.64,

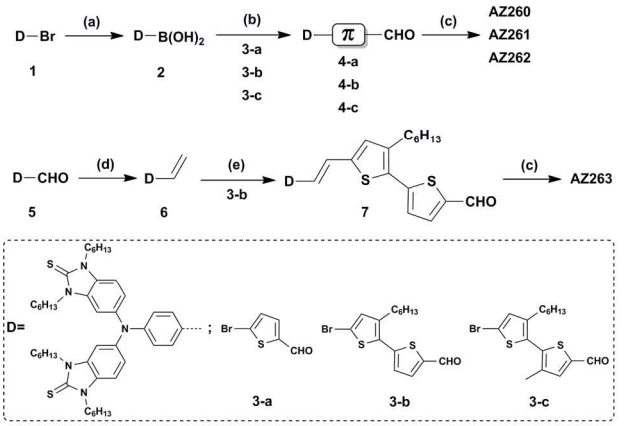

Scheme 1 Synthetic routes of **AZ260-263**. *Reaction conditions*: (a) (1) *n*-BuLi, THF, -78 °C, 1.5 h; (2) $B(OBu)_3$, -78 °C, 2 h; (3) HCl aqueous solution; (b) K_2CO_3 aqueous solution, $Pd(PPh_3)_4$, TBAB, DMF, 75 °C, 2 h; (c) cyanoacetic acid, CH_3COONH_4, CH_3COOH, reflux, 5 h; (d) (1) PPh_3CH_3Br, THF, *t*-BuOK, -10 °C, 2 h; (2) 10 °C, 5 h. (e) $Pd(OAc)_2$, DMF, TBAB, K_2CO_3, reflux, 24 h.

30.46, 30.39, 29.14, 29.00, 28.20, 26.92, 26.79, 25.56, 25.42, 21.56, 21.52, 21.44, 13.06, 13.00, 12.99. MS (ESI) *m/z* calcd. for $C_{64}H_{82}N_6O_2S_4$: 1094.53. Found: 1093.52 ([M-H]$^-$). Anal. Calcd. for $C_{64}H_{82}N_6O_2S_4$: C, 70.16; H, 7.54; N, 7.67. Found: C, 70.09; H, 7.55; N, 7.46.

2.2. UV-Vis measurements

UV-Vis absorption/reflectance spectra were carried out on Shimadzu UV-Vis-NIR Spectrophotometer UV-3600. For the estimation of the dye-loading capacity,[20] the dye adsorbed onto the TiO_2 photoanode was dissolved in a 0.1 g mL^{-1} NaOH solution (H_2O-Ethanol-THF (1:1:1, v/v/v) mixture as the solvent), and its absorption property was characterized using a UV-Vis-NIR Spectrophotometer.

2.3. Electrochemical measurements

The electrochemical cyclic voltammetry was conducted on a CHI 660D Electrochemical Workstation at a scan rate 100 mV s^{-1}, measured in a MeCN-DCM (3:1, v/v) solution containing 0.1 M tetrabutylammonium hexafluorophosphate (Bu_4NPF_6) as a supporting electrolyte (working electrode: glassy carbon; counter electrode: Pt; reference electrode: non-aqueous Ag/Ag$^+$ electrode) under Ar atmosphere. The redox potentials were calibrated with ferrocene/ferrocenium (Fc/Fc$^+$) as the internal reference. Electrical impedance spectra (EIS)[21] for DSSCs under dark with bias -0.7 V were also measured with CHI 660D Electrochemical Workstation at frequencies of 0.05-100000 Hz. The magnitude of the alternative signal was 10 mV. Charge-transfer resistances were determined by fitting the impedance spectra using Z-view software.

2.4. DSSC fabrication and photovoltaic measurements

The glass plates (F-doped SnO_2, 14 M/sq, > 90% transparency in the visible region, Geao, China) were sequentially cleaned in a detergent solution for 30 min, acetone solution for 15 min, deionized water for 15 min using an ultrasonic bath. Then were coated four layers of TiO_2 (20 nm, Geao, China) by screen-printing method. The film was then sequentially sintered at 325 °C for 5 min, 375 °C for 5 min, 450 °C for 15 min, and finally 480 °C for 15 min. The sintered films were then covered with a layer of scattering particle (200 nm spheric particles TiO_2 or 400 nm mesoporous spheres TiO_2), followed by calcination using the above-mentioned method. TiO_2 photoanodes composed of 6.5 μm nanoparticle (20 nm TiO_2) layer in direct contact with the FTO substrate and 3.5 μm light scattering particle (200 nm spheric particles TiO_2 or 400 nm mesoporous spheres TiO_2) layer were fabricated with a screen printing method. The thickness of TiO_2 film was measured by SEM (Quanta 200) and the result was about 10 μm. Upon cooling to room temperature, the TiO_2 photoanodes were immersed in solutions 0.4 mM organic dye solutions in *tert*-butanol-acetonitrile (1:1, v/v) at room temperature for 24 h. The counter electrode was prepared by screen-printing a paste of Pt (Geao, China) on an FTO substrate and sintering at 400 °C under air for 15 min. The dye-adsorbed TiO_2 photoanode and a counter electrode were then assembled into a sealed DSSC cell with a sealant spacer (25 μm, Surlyn 1702) between the two electrode plates. A drop of electrolyte solution [1.0 M 1,2-dimethyl-3-*n*-propylimidazolium iodide (DMPII), 0.1 M LiI, 0.12 M I_2, and 0.5 M 4-*tert*-butylpyridine (TBP) in 3-methoxypropionitrile] was introduced into the cell through a drilled hole via vacuum back-filling. Finally, the hole was sealed using the sealant and a cover glass.

The current density-voltage (*J-V*) characteristics of the DSSCs were measured under illumination with AM 1.5 G solar light from a 300 W xenon lamp solar simulator (94022A, Newport Co., USA). The incident light intensity was calibrated to 100 mW cm^{-2} with a standard Silicon solar cell. *J-V* characteristics were recorded with a digital source meter (Keithley 2400) controlled by a computer. The action spectra of monochromatic incident photon-to-current conversion efficiency (IPCE) for solar cells were tested on a commercial setup (QTest Station 2000 IPCE Measurement System, Crowntech, USA).

3. Results and discussion

3.1. UV-Vis absorption properties

Fig. 2 shows the UV-Vis absorption spectra of the dyes in MeCN-DCM (3:1, v/v) solution and on 6.5 μm TiO_2 films, and the corresponding photophysical data are listed in Table 1. All of the dyes exhibited two distinct absorption bands in solution, one is from the local π-π* absorption in the UV region and the other arises from intramolecular charge transfer (ICT) absorption in the visible region.[22] Compared with **AZ6**, **AZ261** exhibited a blue-shifted of 19 nm in the maximum absorption wavelength (λ_{max}) with a lower molar extinction coefficient (ε), which could be attributed to large steric effect due to the hexyl chain attached to the bithiophene. Further introducing the methyl into the bithiophene, **AZ262** displayed the λ_{max} at 348 nm with an absorption shoulder at around 430 nm due to the weaker ICT absorption overlapped by the π-π* absorption.[17] Obviously, the ICT absorption decreased with the introduction of alkyl chains. However, **AZ260** showed not only blue-shifted in λ_{max} but also low absorption intensity due to the small π-conjugated system caused by the thiophene linker.[23] To further understand the relationship between the length of π-linker and absorption properties, **AZ263** containing a double-bond on the π-linker was compared with **AZ261**, and it was found that the insertion of one double-bond between triphenylamine and bithiophene units resulted in a 26 nm red-shifted in λ_{max} and broadened the absorption band. In addition, the absorption of the dye-coated TiO_2 films also followed the trend of those in solutions but the absorption band red-shifted. Notably, the absorption intensity from 400 to 650 nm were significantly enhanced for all the dyes, which could be explained by the increased delocalization of the π* orbital of the conjugated skeleton caused by the interaction between the carboxylate group and the Ti^{4+} ions, and the energy of the π* level was directly decreased.[24] This is beneficial to

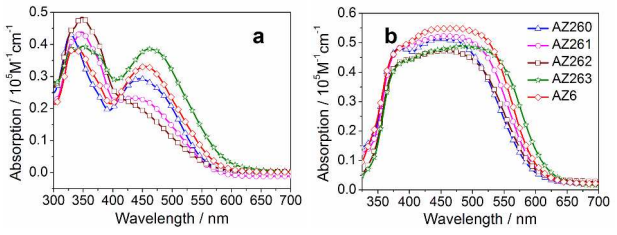

Fig. 2 UV-Vis absorption spectra of **AZ260-263** and **AZ6** in MeCN-DCM (3:1, V/V) solution (a) and on TiO_2 films (b). The absorption of a TiO_2 film has been subtracted for clarity of presentation.

Table 1 Absorption, cyclic voltammetry (CV), and density functional theory (DFT) calculations of **AZ260-263** and **AZ6.**

Dyes	Absorption		CV[c]					DFT[d]				
	λ_{max}/nm (ε/M^{-1} cm^{-1})[a]	λ_{max}/nm (ε/M^{-1} cm^{-1})[b]	E_{ox}/ V	E_{red}/ V	E_{HOMO}/ eV	E_{LUMO}/ eV	E_g^{ec}/ eV	E_{HOMO}/ eV	E_{LUMO}/ eV	E_g/ eV	θ_1/°	θ_2/°
AZ260	445(29300)	449(51300)	0.24	-1.05	-4.96	-3.67	1.29	-5.39	-2.97	2.42	21.90	/
AZ261	436(23200)	464(52200)	0.23	-1.08	-4.95	-3.64	1.31	-5.12	-2.67	2.45	19.31	20.33
AZ262	348(48500)	461(47200)	0.26	-1.00	-4.98	-3.72	1.26	-5.28	-3.02	2.26	21.02	52.93
AZ263	462(38600)	481(48900)	0.21	-1.01	-4.93	-3.71	1.22	-5.12	-2.92	2.20	0.39	19.85
AZ6	455(33100)	472(54900)	0.21	-1.06	-4.93	-3.66	1.27	-5.26	-2.97	2.29	25.36	15.01

[a] Measured in MeCN-DCM (3:1, v/v) solution. [b] Measured on 6.5 μm TiO_2 films.

[c] Measured by cyclic voltammetry (CV) in MeCN-DCM (3:1, v/v) solution.

[d] Calculated by density functional theory (DFT) with the Gaussian 03 program package at the B3LYP/6-311G (d, p) level.

harvest the visible light.

3.2. Electrochemical properties

The redox potentials were measured by cyclic voltammetry (CV) to evaluate the HOMO-LUMO energy levels and the electron transfer process from the excited dye molecule to the conduction band of TiO_2,[25] and the cyclic voltammograms of the dyes are shown in Fig. 3. All of the dyes showed oxidation/re-reduction processes at positive potential range and reduction/oxidation processes at negative potential range, indicating that these dyes have the capability to transport both electrons and holes.[26] The HOMO and LUMO energy levels (E_{HOMO} and E_{LUMO}) as well as the electrochemical energy gap (E_g^{ec}) were calculated from the onset oxidation potentials (E_{ox}) and the onset reduction potentials (E_{red}) by assuming the energy level of ferrocene/ferrocenium (Fc/Fc^+) to be - 4.72 eV below the vacuum level.[27]

The results (Table 1) demonstrated that all of the dyes have sufficiently high E_{LUMO} and are energetically favorable for electron injection into the conduction band of TiO_2 (*ca.* −4.0 eV *vs.* vacuum[28]). The E_{HOMO} also favors the regeneration of the oxidized dye by I^-/I_3^- redox couple (−4.80 eV *vs.* vacuum[29]). **AZ263** showed narrower E_g^{ec} than that of the other dyes, indicating that such molecular architecture would be more beneficial to the electron transfer from the donor to the acceptor.

3.3. Theoretical approach

To theoretically explain the dependence of the absorption properties and the electronic properties on the variations of the linkers, density functional theory (DFT) calculations were conducted using the Gaussian 03 program package at the B3LYP/6-311G(d, p) level,[30,31] and the calculated results are also recorded in Table 1.

From the optimized geometry (Fig. 4) of **AZ260**, **AZ261**, **AZ262** and **AZ6**, the dihedral angles between the phenyl and the adjacent thiophene (θ_1) were calculated to be in the range from 19º to 26º. As for **AZ263**, however, it was found that the phenyl was entirely in plane with the thiophene due to the insertion of the double-bond between them. This planar configuration maximized the π-conjugation pathway throughout the whole molecule[32] and brought a remarkably red-shifted in the maximum absorption band, which is in line with the UV-Vis absorption spectra discussed above. The dihedral angle between the thiophene and the adjacent thiophene (θ_2) in **AZ6**, **AZ261**, and **AZ262** are 15.01º, 20.33º and 52.93º, respectively. Obviously, **AZ261** and **AZ262** exhibites more twisted dihedral angles due to the introduction of the hexyl and the methyl with large steric effect, which results in a blue-shifted of the maximum absorption band.[2,17] Nevertheless, the detrimental blue shift could be compensated by the augment of a double-bond into the π-linker.[18]

As shown in Fig. 5, the HOMO and LUMO perfectly revealed that the donor-acceptor character of the cyclic thiourea functionalized triphenylamine and the anchoring groups. Such dye architecture provides an energy gradient for the excitation and facilitated the HOMO to LUMO charge transfer transition, which is crucial to afford a favorable energetic pathway for electron injection into the conduction band of TiO_2.[32] A closer look at the calculated E_{HOMO} and E_{LUMO} revealed the impact of the subtle variations of molecular structure in these systems. **AZ260** and **AZ6** have the same E_{LUMO}, but the E_{HOMO} of the latter is much higher than that of the former along with the extension of conjugation length. Although **AZ261** and **AZ262** contain the same conjugated skeleton as **AZ6**, the hexyl chain attached to the bithiophene induced the increase of the E_{HOMO} and E_{LUMO} of **AZ261**; however, continuing to introduce the methyl to

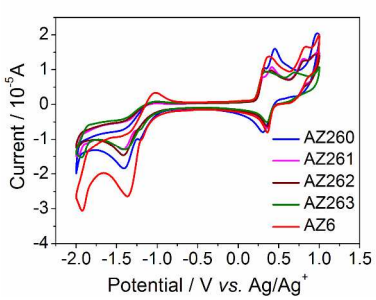

Fig. 3 Cyclic voltammograms of **AZ260-263** and **AZ6**.

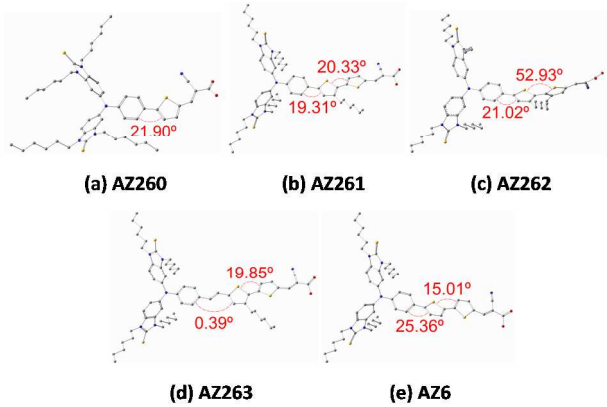

Fig. 4 Dihedral angles between phenyl and adjacent thiophene or thiophene and adjacent thiophene of (a) **AZ260**, (b) **AZ261**, (c) **AZ262**, (d) **AZ263**, and (e) **AZ6**.

Table 2 Correlation of the photovoltaic performance with the dye-loading capacity of three distinct photoanodes: **NC**, **NC-SP200**, and **NC-MS400**.

Photoanode	J_{sc}/mA cm^{-2}	V_{oc}/mV	FF	PCE/%	Absorbed dye (10^{-7}mol cm^{-2})[a]
NC	13.16	749.5	0.639	6.31	1.60
NC-SP200	14.52	749.5	0.638	6.94	1.74
NC-MS400	15.94	739.4	0.624	7.35	2.18

[a] Dye-adsorbed films with a dimension of 0.25 cm^2 were used for estimating the adsorbed dye concentration.

the bithiophene resulting in the decrease of the E_{HOMO} and E_{LUMO} of **AZ262**. **AZ263** displayed a lower E_{LUMO} than that of **AZ261**, but the E_{HOMO} of both showed no changes, which could be ascribed to the enhancement of the conjugated linker through the insertion of one double-bond. In addition, compared the E_{HOMO} and E_{LUMO} of **AZ263** with those of **AZ6**, the results showed that the introduction of one double-bond and a hexyl chain into the π-linker not only drove up the HOMO level but also drove down the LUMO level, resulting in a narrow energy gap (E_g). It is worthy of note that the E_g from the DFT calculation is bigger than the E_g^{ec} from the experiment, which is a common feature of organic optoelectronic materials and may be related to the solvent effect;[33,34] but the relationship between them is linear (Fig. S1).

3.4. Photoanode effect on photovoltaic performance

To validate the effect of the photoanode on the photovoltaic performance, 200 nm spheric particles TiO_2 (labeled **SP200)** and 400 nm mesoporous spherical TiO_2 film (labeled **MS400**) as scattering layers were respectively coated on 20 nm nanocrystalline TiO_2 film (labeled **NC**), which formed bilayered **NC-SP200** film and **NC-MS400** film as the photoanodes. In order to further insight into the photoanodes, the morphology (ESI†), physical properties and dye-loading capacities were investigated.

Fig. 6a and b show the diffuse reflectance spectra of **NC**, **SP200**, and **MS400** without and with **AZ261**. It was observed that the reflectance in the visible region decreased in the order of **SP200** > **MS400** > **NC**. The reflectance of **NC** with **AZ261** was almost less than 5%, which indicates that it barely reflects the incident light. The absorption spectra (Fig. 6c and d) demonstrated that **SP200** changed less before and after loading **AZ261**, while **NC** and **MS400** changed more. It is worth noting that the absorption intensity of **NC** with **AZ261** is markedly enhanced in the range from 400 nm to 650 nm. As shown in Fig. 6e, the absorption intensity represents the dye-loading capacity of the TiO_2 film (**NC** > **MS400** > **SP200**),[35,36] which corresponds to the actual objects (Fig. 6f). Obviously, the scattering layer **MS400** plays an assistant role in loading dye. The merit of **MS400** as the scattering layer can be elaborated by the schematic diagrams (Fig. S3). Some of the incident light is lost when passes through the absorbing layer **NC**, which can be reflected back into the nanocrystalline TiO_2 film by **SP200** and **MS400**. To further quantify the dye-loading capacity of **NC**, **NC-SP200**, and **NC-MS400**, desorption experiments (ESI†) were carried out, and the results are summaried in Table 2. Compared with **NC**, **NC-SP200** increased by 8.75%, while **NC-MS400** increased by 36.25%.

The *J-V* characteristics of **AZ261** based on three distinct photoanodes are shown in Fig. S5. The photovoltaic performance parameters were summarized in Table 2. Obviously, the **NC** cell shows the lowest PCE of 6.31% with a J_{sc} as low as 13.16 mA cm^{-2}. For **NC-SP200** cell, the J_{sc} is significantly enhanced to 14.52 mA cm^{-2} with a PCE of 6.94%. Moreover, the J_{sc} of **NC-**

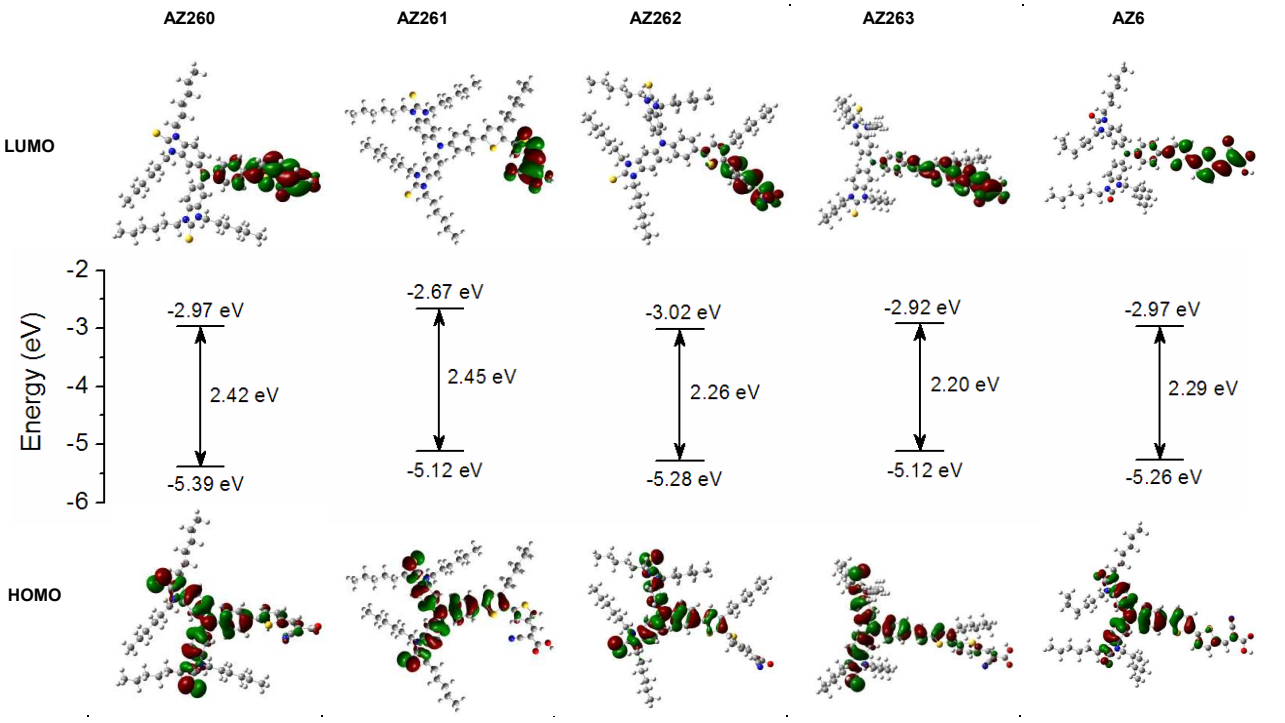

Fig. 5 The frontier orbitals and energy levels of **AZ260-263** and **AZ6** by DFT calculations.

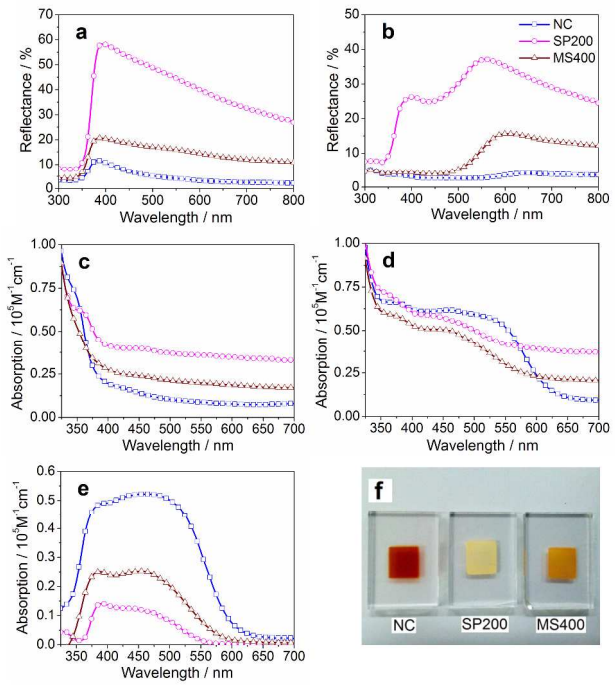

Fig. 6 Diffuse reflectance spectra of **NC**, **SP200**, and **MS400** without (a) and with (b) **AZ261**; the corresponding absorption spectra without (c) and with (d) **AZ261**; absorption spectra (e) of the TiO_2 reference film was subtracted for clarity; photo of **NC**, **SP200**, and **MS400** with **AZ261** (f).

MS400 cell is significantly enhanced to 15.94 mA cm^{-2} with a PCE of 7.35%, which is ascribed to the combined effect of relatively high specific surface area of the mesoporous spherical TiO_2[37] and light-scattering. Therefore, it is reasonable to conclude that the **NC-MS400** cell provides the optimal dual effects of the highest dye loading and optical confinement, resulting in a noticeable improvement of J_{sc} and PCE.

3.5. Photovoltaic performance measurements

The *J-V* characteristics and IPCE spectra of the dyes based on **NC-MS400** photoanode are shown in Fig. 7a and b. The corresponding photovoltaic data are collected in Table 3.

The J_{sc} values increased in the order: **AZ260** (13.91 mA cm^{-2}) < **AZ262** (15.02 mA cm^{-2}) < **AZ6** (15.89 mA cm^{-2}) < **AZ261** (16.02 mA cm^{-2}) < **AZ263** (17.83 mA cm^{-2}). The values of J_{sc} are closely related to the integral of the IPCE spectra. For example, **AZ260** with only one thiophene as the π-linker afforded the lowest J_{sc} because of the narrowest spectral response and lowest IPCE maximum (71.05% at 490 nm) among these dyes. A comparison of **AZ6** with **AZ260** demonstrated that the merit of employing bithiophene is to enhance light-harvesting and improve the photocurrent.[13] Although **AZ261**, **AZ262**, and **AZ6** contained the same π-conjugated skeleton, **AZ261** displayed a relatively high J_{sc}. This could be mainly attributed to its coplanar structure.[24] However, **AZ262** showed a relatively low J_{sc} in spite of the highest IPCE maxima (83.50% at 490 nm). This phenomenon could be explained by its spectral limitation caused by the twisted structure. Among these dyes, **AZ263** gave rise to the highest J_{sc} because electrons could be more easily transferred through the coplanar structure into the TiO_2,[22] moreover, the planar configuration causes a remarkably broadening absorption

Table 3 Photovoltaic performance data of **AZ260-263** and **AZ6**.

Dye	J_{sc}/mA cm^{-2}	V_{oc}/mV	FF	PCE/%	IPCE/% (λ_{max}/nm)
AZ260	13.91	709.0	0.68	6.73	71.05 (490)
AZ261	16.02	739.4	0.63	7.42	80.01 (500)
AZ262	15.02	749.4	0.61	6.91	83.50 (490)
AZ263	17.83	719.2	0.64	8.24	76.20 (520)
AZ6	15.89	729.2	0.62	7.20	78.71 (510)

band, which is beneficial to the improvement of light-harvesting capacity.[24] In addition, the IPCE spectrum of **AZ263** exhibited a significantly larger area than the others.

The V_{oc} values increased in the order: **AZ260** (709.0 mV) < **AZ263** (719.2 mV) < **AZ6** (729.2 mV) < **AZ261** (739.4 mV) < **AZ262** (749.4 mV). The EIS was investigated to further elucidate the V_{oc} results and obtain more interfacial charge transfer information. In the Nyquist plots (Fig. 7c), the larger semicircle in the low frequency region corresponds to charge-transfer resistance (R_{rec}) at the TiO_2/dye/electrolyte interface; e.g., a larger radius indicates a larger R_{rec} and slower electron recombination. In addition, the electron lifetime could be calculated from the Bode phase plots (Fig. 7d).[38] The calculated results increased in the order of **AZ260** (21.1 ms) < **AZ263** (21.8 ms) < **AZ6** (24.5 ms) < **AZ261** (29.5 ms) < **AZ262** (32.2 ms). Both the R_{rec} and electron lifetime coincided well with V_{oc}. The enlarged R_{rec} and lengthened τ_e further indicated that the electron recombination between the injected electrons and the electrolyte was decreased, resulting in an increased V_{oc}.[38] Under the same π-conjugated conditions, the V_{oc} gradually increases with the introduction of alkyl substituents into π-linkers (**AZ6** < **AZ261** < **AZ262**). This is because the twisted nonplanar structures can reduce intermolecular aggregation[22] and suppress the electron recombination.[24,39] However, **AZ263** showed a lower V_{oc} than **AZ261** because of the introduction of one double-bond in **AZ263** resulting in the narrower E_g as mentioned above,[40] or a faster electron recombination.

The differences of PCE are caused by the different J_{sc} and V_{oc}. Among these DSSC devices, DSSC based on **AZ260** delivered a poor PCE of 6.73% due to its lowest J_{sc} and V_{oc}. In comparison

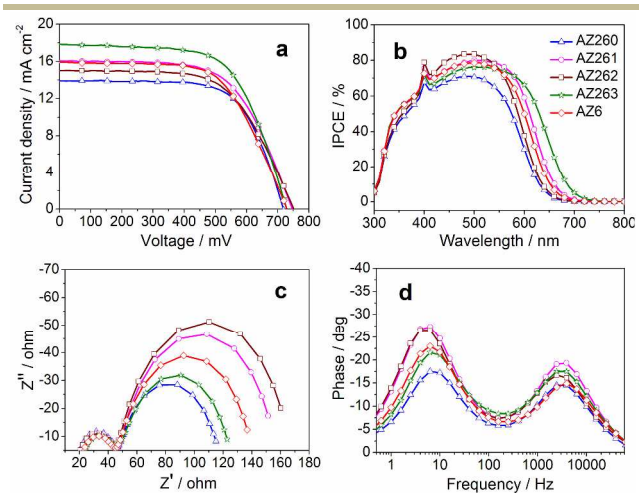

Fig. 7 (a) *J-V* characteristics and (b) IPCE spectra for DSSCs based on **AZ260-263** and **AZ6**; the corresponding EIS spectra: (c) Nyquist and (d) Bode phase plots.

with **AZ6**, **AZ261** offered relatively high J_{sc} and V_{oc}, resulting in a higher PCE of 7.42%. However, **AZ262** yielded a lower PCE of 6.91% due to the lower J_{sc} caused by the narrower IPCE spectra.[41] Encouragingly, the DSSC from **AZ263** with the highest J_{sc} of 17.83 mA cm^{-2}, which overwhelms the unfavorable effect of V_{oc}, exhibited a PCE as high as 8.24%.

4. Conclusions

In summary, four cyclic thiourea functionalized dyes have been synthesized and their DSSC performances were evaluated as well. On the premise of coplanar structure, the absorption bands were broadened by increasing the length of π-conjugated linker, e.g. the augmentation of the conjugated thiophene number or the insertion of the double-bond, which can enhance the light-harvesting and improve the J_{sc}. The steric hindrance of the dye molecule was efficiently increased by introducing alkyl substituents into the bithiophene linker, which can suppress the intermolecular π-π aggregation and the electron recombination, resulting in an increased V_{oc}. Moreover, a comparison of **AZ263** with **AZ6** showed that the introduction of one double-bond along with a hexyl chain into the π-linker not only drove up the HOMO level but also drove down the LUMO level, resulting in the improvement of J_{sc}. In addition, the double-layered photoanode (**NC-MS400**) with 400 nm mesoporous spherical TiO_2 film as the scattering layer provided the optimal dual effects of the highest dye-loading and optical confinement, resulting in a noticeable improvement of J_{sc}. Our systematical investigation of the J_{sc} and V_{oc} from two aspects of π-linker modification and photoanode selection will have a wealth of opportunity for designing new efficient organic dyes and optimizing DSSCs' performance.

Acknowledgements

This work was supported by the Fundamental Research Funds for the Central Universities (No. GK201304005) and the Natural Science Foundation of China (No. 51373092). Our special thanks are also for the Fund of New Engergy Devices and Materials provided by Mr. He Chong Ben, Hong Kong. We are grateful to Professor Wenliang Wang at Shaanxi Normal University for theoretical calculations. We also thank Minister Chao Gao and Miss Haimei Wu at Xi'an Modern Chemistry Research Institute for electrochemical measurements.

References

1 (a) B. O'Regan and M. Grätzel, *Nature*, 1991, **353**, 737-740; (b) M. Grätzel, *Nature*, 2001, **414**, 338-344.
2 W. H. Nguyen, C. D. Bailie, J. Burschka, T. Moehl, M. Grätzel, M. D. McGehee and A. Sellinger, *Chem. Mater*., 2013, **25**, 1519-1525.
3 (a) R. Chen, X. Yang, H. Tian, X. Wang, A. Hagfeldt and L. Sun, *Chem. Mater*., 2007, **19**, 4007-4015; (b) C.-H. Chen, Y.-C. Hsu, H.-H. Chou, K. R. J. Thomas, J. T. Lin and C.-P. Hsu, *Chemistry*, 2010, **16**, 3184-3193.
4 (a) W. Zeng, Y. Cao, Y. Bai, Y. Wang, Y. Shi, M. Zhang, F. Wang, C. Pan and P. Wang, *Chem. Mater*., 2010, **22**, 1915-1925; (b) Y. Bai, J. Zhang, D. Zhou, Y. Wang, M. Zhang and P. Wang, *J. Am. Chem. Soc.*, 2011, **133**, 11442-11445; (c) G. Zhang, H. Bala, Y. Cheng, D. Shi, X. Lv, Q. Yu and P. Wang, *Chem. Commun.*, 2009, 2198-2200.
5 A. Hagfeldt, G. Boschloo, L. Sun, L. Kloo and H. Pettersson, *Chem. Rev.*, 2010, **110**, 6595-6663.
6 M. Grätzel, *Acc. Chem. Res*., 2009, **42**, 1788-1798.
7 H. Imahori, T. Umeyama and S. Ito, *Acc. Chem. Res*., 2009, **42**, 1809-1818.
8 B. C. O'Regan, I. López-Duarte, M. V. Martinez-Diaz, A. Forneli, J. Albero, A. Morandeira, E. Palomares, T. Tomás and J. R. Durrant, *J. Am. Chem. Soc.*, 2008, **130**, 2906-2907.
9 H. Ellis, S. K. Eriksson, S. M. Feldt, E. Gabrielsson, P. W. Lohse, R. Lindblad, L. Sun, H. Rensmo, G. Boschloo and A. Hagfeldt, *J. Phys. Chem. C*, 2013, **117**, 21029-21036.
10 B. C. O'Regan, K. Walley, M. Juozapavicius, A. Anderson, F. Matar, T. Ghaddar, S. M. Zakeeruddin, C. Klein and J. R. Durrant, *J. Am. Chem. Soc*., 2009, **131**, 3541-3548.
11 Z. Wu, Z. An, X. Chen and P. Chen, *Org. Lett.*, 2013, **15**, 1456-1459.
12 S. Kim, J. K. Lee, S. O. Kang, J. Ko, J.-H. Yum, S. Fantacci, F. D. Angelis, D. D. Censo, M. K. Nazeeruddin and M. Grätzel, *J. Am. Chem. Soc.*, 2006, **128**, 16701-16707.
13 J. Liu, R. Li, X. Si, D. Zhou, Y. Shi, Y. Wang, X. Jing and P. Wang, *Energy Environ. Sci.*, 2010, **3**, 1924-1928.
14 (a) N. Koumura, Z.-S. Wang, S. Mori, M. Miyashita, E. Suzuki and K. Hara, *J. Am. Chem. Soc.*, 2006, **128**, 14256-14257; (b) K. Hara, K. Miyamoto, Y. Abe and M. Yanagida, *J. Phys. Chem. B*， 2005, **109**, 23776-23778.
15 Y. Wu, M. Marszalek, S. M. Zakeeruddin, Q. Zhang, H. Tian, M. Grätzel and W. Zhu. *Energy Environ. Sci.*, 2012, **5**, 8261-8272.
16 (a) Z.-S. Wang, N. Koumura, Y. Cui, M. Takahashi, H. Sekiguchi, A. Mori, T. Kubo, A. Furube and K. Hara, *Chem. Mater.*, 2008, **20**, 3993-4003; (b) Z. Ning, Q. Zhang, H. Pei, J. Luan, C. Lu, Y. Cui and H. Tian, *J. Phys. Chem. C*, 2009, **113**, 10307-10313; (c) Z. Ning, Y. Fu and H. Tian, *Energy Environ. Sci.*, 2010, **3**, 1170-1181; (d) J. Liu, X. Yang, J. Zhao and L. Sun, *RSC Adv*., 2013, **3**, 15734-15743.
17 X. Lu, Q. Feng, T. Lan, G. Zhou and Z.-S. Wang, *Chem. Mater.*, 2012, **24**, 3179-3187.
18 J. Liu, D. Zhou, M. Xu, X. Jing and P. Wang, *Energy Environ. Sci*., 2011, **4**, 3545-3551.
19 Y.-C. Park, Y.-J. Chang, B.-G. Kum, E.-H. Kong, J. Y. Son, Y. S. Kwon. T. Park and H. M. Jang, *J. Mater. Chem.*, 2011, **21**, 9582-9586.
20 L. Yang and W. W.-F. Leung, *RSC Adv*., 2013, **3**, 25707-25710.
21 (a) F. Fabregat-Santiago, J. Bisquert, G. Garcia-Belmonte, G. Boschloo and A. Hagfeldt, *Sol. Energy Mater. Sol. Cells*, 2005, **87**, 117-131; (b) Q. Wang, J.-E. Moser and M. Grätzel, *J. Phys. Chem. B*, 2005, **109**, 14945-14953.
22 S. H. Kim, H. W. Kim, C. Sakong, J. Namgoong, S. W. Park, M. J. Ko, C. H. Lee, W. I. Lee and J. P. Kim, *Org. Lett*., 2011, **13**, 5784-5787.
23 R. Li, X. Lv, D. Shi, D. Zhou, Y. Cheng, G. Zhang and P. Wang, *J. Phys. Chem. C*, 2009, **113**, 7469-7479.
24 T. Duan, K. Fan, C. Zhong, X. Chen, T. Peng and J. Qin, *J. Power Sources*, 2013, **234**, 23-30.
25 L. Yu, J. Xi, H. T. Chan, T. Su, L. J. Antrobus, B. Tong, Y. Dong, W. K. Chan and D. L. Phillips, *J. Phys. Chem. C*, 2013, **117**, 2041-2052.
26 Q. Sun, H. Wang, C. Yang and Y. Li, *J. Mater. Chem.*, 2003, **13**, 800-806.
27 (a) J. Hou, Z. Tan, Y. Yan, Y. He, C. Yang and Y. Li, *J. Am. Chem. Soc.*, 2006, **128**, 4911-4916; (b) Y. Lu, Z. Xiao, Y. Yuan, H. Wu, Z. An, Y. Hou, C. Gao and J. Huang, *J. Mater. Chem. C*, 2013, **1**, 630-637.
28 (a) Y. S. Kwon, J. Lim, I. Song, I. Y. Song, W. S. Shin, S.-J. Moon and T. Park, *J. Mater. Chem.*, 2012, **22**, 8641-8648; (b) J. B. Asbury, Y.-Q. Wang, E. Hao, H. N. Ghosh and T. Lian, *Res. Chem. Intermed.*, 2001, **27**, 393-406.
29 D. Cahen, G. Hodes, M. Grätzel, J. F. Guillermoles and I. Riess, *J. Phys. Chem. B*, 2000, **104**, 2053-2059.
30 M. J. Frisch, G. W. Trucks, H. B. Schlegel, G. E. Scuseria, M. A. Robb, J. R. Cheeseman, V. G. Zakrzewski, J. A. Jr. Montgomery, R. E. Stratmann, J. C Burant, J. M. Millam, S. S. Iyengar, J. Tomasi, V. Barone, B. Mennucci, M. Cossi, G. Scalmani, M. Rega, G. A. Petersson, H. Nakatsuji, M. Hada, M. Ehara, K. Toyota, R. Fukuda, J. Hasegawa, M. Ishida, T. Nakajima, Y. Honda, O. Kitao, H. Nakai, M. Klene, X. Li, J. E. Knox, H. P. Hratchain, J. B. Cross, V. Bakken, C. Adamo, J. Jaramillo, R. Gomperts, R. E. Stratmann, O. Yazyev, A. J. Austin, R. Cammi, C. Pomelli, J. W. Ochterski, P. Y. Ayala K. Morokuma,; G. A. Voth, P. Salvador, J. J. Dannenberg, V. G.

Zakrzewski, S. Dapprich, A. D. Danniels, M. C. Strain, O. Farkas, D. K. Malick, A. D. Rabuck, K. Raghavachari, J. B. Foresman, J. V. Ortiz, Q. Cui, A. G. Baboul, S. Clifford, J. Cioslowski, B. B. Stefanov, G. Liu, A. Liashenko, P. Piskorz, I. Komaroni, R. L. Martin, D. L. Fox, T. Keith, M. A. Al-Laham, C. Y. Peng, A. Nanayakkara, M. Challacombe, P. M. W. Gill, B. Johnson, W. Chen, M. W. Wong, C. Gonzalez, and J. A. Pople, *Gaussian 03, Revision C. 02*, Gaussian, Inc., Wallingford CT, 2004.

31 (a) C. Lee, W. Yang and R. G. Parr, *Phys. Rev. B.*, 1988, **37**, 785-789; (b) A. D. McLean and G. S. Chandler, *J. Chem. Phys.*, 1980, **72**, 5639-5648.

32 M. Katono, T. Bessho, M. Wielopolski, M. Marszalek, J.-E. Moser, R. Humphry-Baker, S. M. Zakeeruddin and M. Grätzel, *J. Phys. Chem. C*, 2012, **116**, 16876-16884.

33 G. Zhang, Y. Bai, R. Li, D. Shi, S. Wenger, S. M. Zakeeruddin, M. Grätzel and P. Wang, *Energy Environ. Sci.*, 2009, **2**, 92-95.

34 M. Heeney, W. Zhang, D. J. Crouch, M. L. Chabinyc, S. Gordeyev, R. Hamilton, S. J. Higgins, I. McCullouch, P. J. Skabara, D. Sparrowe and S. Tierney, *Chem. Commun*., 2007, **47**, 5061-5063.

35 X. Sun, Y. Liu, Q. Tai, B. Chen, T. Peng, N. Huang, S. Xu, T. Peng and X.-Z. Zhao, *J. Phys. Chem. C*, 2012, **116**, 11859-11866.

36 S. Wu, H. Han, Q. Tai, J. Zhang, S. Xu, C. Zhou, Y. Yang, H. Hu, B. Chen and X.-Z. Zhao, *J. Power Sources*, 2008, **182**, 119-123.

37 J. Y. Ahn, K. J. Moon, J. H. Kim, S. H. Lee, J. W. Kang, H. W. Lee and S. H. Kim, *ACS Appl. Mater. Interfaces*, 2014, **6**, 903-909.

38 Z. Wan, C. Jia, Y. Duan, L. Zhou, Y. Lin and Y. Shi, *J. Mater. Chem.*, 2012, **22**, 25140-25147.

39 M. Velusamy, K. R. J. Thomas, J. T. Lin, Y.-C. Hsu and K.-C. Ho, *Org. Lett.*, 2005, **7**, 1899-1902.

40 (a) V. D. Mihailetchi, P. W. M. Blorn, J. C. Hummelen and M. T. Rispens, *J. Appl. Phys.*, 2003, **94**, 6849-6854; (b) V. Dyakonov, *Appl. Phys. A*, 2004, **79**, 21-25.

41 D. P. Hagberg, J.-H. Yum, H. J. Lee, F. D. Angelis, T. Marinado, K. M. Karlsson, R. Humphry-Baker, L. Sun, A. Hagfeldt, M. Grätzel and M. K. Nazeeruddin, *J. Am. Chem. Soc.*, 2008, **130**, 6259-6266.

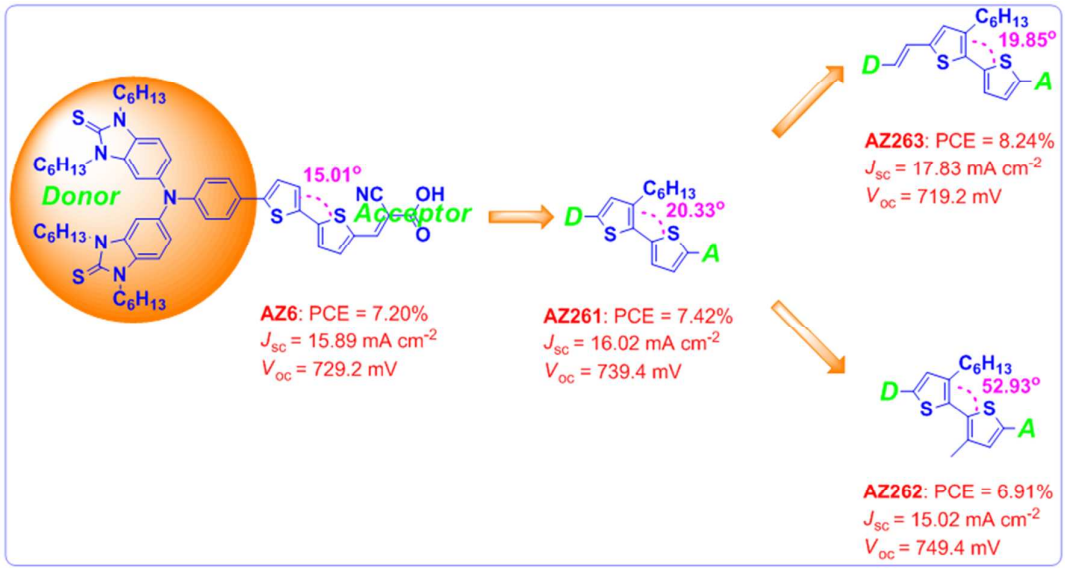

Modification of the π-linker of cyclic thiourea functionalized dyes have a significant effect on the short-circuit current and open-circuit voltage of dye-sensitized solar cells.